Mechanics of Advanced Composite Structures 1 (2014) 49 – 60

Semnan University

Mechanics of Advanced Composite Structures

journal homepage: http://MACS.journals.semnan.ac.ir

Elasticity Solution of Functionally Graded Carbon Nanotube Reinforced Composite Cylindrical Panel

A. Alibeigloo*

Department of Mechanical Engineering, Tarbiat Modares University, Tehran, 14115-143, Iran

PAPER INFO

Paper history:
Received 7 August 2014
Received in revised form 7 September 2014
Accepted 24 September 2014

Keywords:
Carbon nanotube
Cylindrical panel
Boundary layer
Static
Elasticity

ABSTRACT

Based on three-dimensional theory of elasticity, static analysis of functionally graded carbon nanotube reinforced composite (FG-CNTRC) cylindrical panel subjected to mechanical uniformed load with simply supported boundary conditions is carried out. In the process, stress and displacement fields are expanded according to the Fourier series along the axial and circumferential coordinates. From constitutive law, stress-displacement relations and equilibrium equations, state space equation is obtained. The obtained first order governing differential equations can be solved analytically. The effects of CNT distribution cases, the volume fraction of CNT, length to mid radius ratio, span of the cylindrical panel, variation of mechanical load and radius to thickness ratio on the bending behaviour of the cylindrical panel are examined. It should be noted that by using Fourier series solution it is possible only to solve the static behaviour of cylindrical panel with simply supported for all of edges and for the non-simply supported boundary conditions it is possible to solve numerically. The obtained analytical solution can be used to validate the results of approximate two dimensional conventional theories.

1. Introduction

The high strength and stiffness of carbon nanotubes cause to use them as reinforcing constituents instead of conventional fibers in composite structures such as beam, plate and shell. The introduction of CNT into polymer matrix increases the application of reinforcing composite. Study on the mechanical and thermal properties of CNTRC structures has increased by many researchers in recent years. Thostenson et al. [1] presented a review on the researches and application of CNT and CNTRC. Gou et al. [2] used the molecular dynamics (MD) simulations and experimental method to investigate the interfacial bonding of single-walled nanotube (SWNT) reinforced epoxy composites. Wuite and Adali [3] carried out a multi scale analysis of the deflection and stress behaviour of carbon nanotube (CNT) reinforced polymer composite beams. Vodenitcharova and Zhang [4] investigated pure bending and bending-induced local buckling of a nanocomposite beam reinforced by a SWNT computationally as well as experimentally using Airy stress-function approach. Shen [5] discussed nonlinear bending behaviour of simply supported and functionally graded composite plates reinforced by SWCNTs subjected to transverse uniformed or sinusoidal load in thermal environments. Formica et al. [6] used an equivalent continuum model and Eshelby–Mori–Tanaka approach to study the vibrational behaviour of CNTRC. By using multi-scale approach, Shen and Zhang [7] discussed thermal buck-

* Corresponding author. +98-21-82883991; Fax: +98-21-82884909

E-mail address: abeigloo@modares.ac.ir

ling and post buckling behaviour of functionally graded nanocomposite plates reinforced by SWCNTs subjected to in-plane temperature variation. Based on Timoshenko beam theory and von Karman geometric nonlinearity, Ke et al. [8] discussed nonlinear free vibration of FG nanocomposite beams reinforced by SWCNTs by using Ritz method. Shen [9] used higher order shear deformation theory as well as a von Kármán-type of kinematic nonlinearity to investigate the post buckling behaviour of nanocomposite cylindrical shells reinforced by SWCNTs and subjected to axial environments. Based on a micromechanical model and multi-scale approach, Shen [10] discussed post buckling behaviour of FG-CNTRC cylindrical shells subjected to mechanical load in thermal environments. Based on a higher order shear deformation plate theory, Wanga and Shen [11] investigated the nonlinear vibration of FG-SWCNT plates rested on elastic foundation in thermal environments by using an improved perturbation technique. Mehrabadi et al. [12] discussed mechanical buckling behaviour of FG nanocomposite plate reinforced by SWCNTs by using Mindlin plate theory based on first-order shear deformation (FSDT). Zhu et al. [13] carried out bending and free vibration analysis of composite plates reinforced by SWCNTs by using the finite element method based on the first order shear deformation plate theory. Wang and Shen [14] investigated nonlinear bending and vibration behaviour of sandwich plate with CNTRC face sheets by using multi-scale approach and two-step perturbation technique. Yas and Heshmati [15] used Timoshenko beam theory to analysis the vibration of FG nanocomposite beams reinforced by randomly oriented straight SWCNTs subjected to moving load. Recently the author [16] presented an analytical solution for bending behaviour of FG-CNT composite plate integrated with piezoelectric actuator and sensor under an applied electric field and mechanical load. Bhardwaj et al. [17] investigated the non-linear static and dynamic behaviour of cross-ply CNTRC laminated plate by using the double Chebyshev series. By using higher order shear deformation theory and Von Karman type of kinematic nonlinearity, Shen [18] discussed post buckling of FG-CNTRC cylindrical shell in thermal environment. Nonlinear vibration of FG-CNTRC cylindrical shell was investigated by Shen and Xiang [19] using the equation of the motion based on higher-order shear deformation theory with a Von Karman-type of kinematic nonlinearity. Moradi-Dastjerdi et al. [20] analysed the dynamic behaviour of FG-CNTRC cylindrical shell subjected to impact load by making the use of mesh free method. By using Eshelby–Mori–Tanaka approach and two-dimensional differential quadrature method, free vibration analysis of CNTRC cylindrical panel was presented by Sobhani Aragh [21]. According to the above mentioned research it is seen that static analysis of FG-CNTRC cylindrical panel has not been yet considered. In this paper, based on the theory of elasticity, bending behaviour of FG-CNTRC cylindrical panel subjected to uniformed internal pressure is studied.

2. Basic Equations

2.1. FG-CNTRC Layer

A CNTRC cylindrical panel with geometry and dimensions according to the Fig.1 is considered. The SWCNT reinforcement is either uniformly distributed (UD) or functionally graded (FG) in four cases, *FG-V*, $FG-\Lambda$, $FG-X$ and $FG-O$ in the thickness direction. Displacements component along the r, θ and z directions are denoted by u_r, u_θ and u_z, respectively. According to the rule of mixture and considering the CNT efficiency parameters, the effective mechanical properties of mixture of CNTs and isotropic polymer matrix can be written as the following [6]

$$E_{11} = \eta_1 \mathrm{V}_{CN} \mathrm{E}_{11}^{CN} + \mathrm{V}_m \mathrm{E}^m \tag{1.1}$$

$$\frac{\eta_2}{E_{22}} = \frac{V_{CN}}{E_{22}^{CN}} + \frac{V_m}{E^m} \tag{1.2}$$

$$\frac{\eta_3}{G_{12}} = \frac{V_{CN}}{G_{12}^{CN}} + \frac{V_m}{G^m} \tag{1.3}$$

The relation between the CNT and matrix volume fractions is stated as:

$$V_{CN} + V_m = 1 \tag{2}$$

The volume fraction of CNT for five cases *UD*, *FG-V*, $FG-\Lambda$, $FG-X$ and $FG-O$ distribution along the thickness according to the Fig.1 has the following relations, respectively:

$$V_{CNT} = V_{CNT}^* \tag{3.1}$$

$$V_{CNT} = 2\left(\frac{r-R}{h} + 0.5\right) V_{CNT}^* \tag{3.2}$$

$$V_{CNT} = 2\left(-\frac{r-R}{h} + 0.5\right) V_{CNT}^* \tag{3.3}$$

$$V_{CNT} = 4 \times \frac{|r-R|}{h} V_{CNT}^* \tag{3.4}$$

$$V_{CNT} = 4\left(0.5 - \frac{|r-R|}{h}\right)V_{CNT}^{*} \tag{3.5}$$

where R is mid-radius of the panel and

$$V_{CNT}^{*} = \frac{W_{CN}}{W_{CN} + \left(\frac{\rho_{CN}}{\rho_m}\right) - \left(\frac{\rho_{CN}}{\rho_m}\right)W_{CN}} \tag{3.6}$$

The Poisson's ratio, ν_{12} and the density of the nanocomposite panel is assumed as:

$$\nu_{12} = V_{CNT}^{*}\nu_{12}^{CNT} + V_m\nu^m \tag{4.1}$$

$$\rho = V_{CNT}\rho^{CNT} + V_m\rho^m \tag{4.2}$$

And the other effective mechanical properties of mixture of CNTs and isotropic polymer matrix are:

$$E_{33} = E_{22}\ ,\ G_{12} = G_{13} = G_{23}\ ,\ \nu_{13} = \nu_{12}\ ,\ \nu_{31} = \nu_{21}$$

$$\nu_{32} = \nu_{23} = \nu_{21}\ ,\ \nu_{12} = \frac{E_{22}}{E_{11}}\nu_{12}$$

The constitutive equations for CNTRC panel layer are written as:

$$\sigma = \mathrm{Q}\varepsilon \tag{5}$$

where

$$\sigma = \left\{\sigma_z \quad \sigma_\theta \quad \sigma_r \quad \tau_{r\theta} \quad \tau_{zr} \quad \tau_{z\theta}\right\}^{\mathrm{T}}$$

$$\varepsilon = \left\{\varepsilon_z \quad \varepsilon_\theta \quad \varepsilon_r \quad \gamma_{r\theta} \quad \gamma_{zr} \quad \gamma_{z\theta}\right\}^{\mathrm{T}}$$

$$Q = \begin{bmatrix} Q_{11} & Q_{12} & Q_{13} & 0 & 0 & 0 \\ Q_{12} & Q_{22} & Q_{23} & 0 & 0 & 0 \\ Q_{13} & Q_{23} & Q_{33} & 0 & 0 & 0 \\ 0 & 0 & 0 & Q_{44} & 0 & 0 \\ 0 & 0 & 0 & 0 & Q_{55} & 0 \\ 0 & 0 & 0 & 0 & 0 & Q_{66} \end{bmatrix}$$

And the relation between the stiffness elements, Q_{ij} and engineering constants E_{ij}, G_{ij} and ν_{ij} are described in the appendix. In the absence of body forces, the governing equilibrium equations in three dimensions are:

$$\frac{\partial\sigma_r}{\partial r} + \frac{\partial\tau_{zr}}{\partial z} + \frac{1}{r}\frac{\partial\tau_{r\theta}}{\partial\theta} + \frac{1}{r}\left(\sigma_r - \sigma_\theta\right) = 0$$

$$\frac{\partial\tau_{r\theta}}{\partial r} + \frac{\partial\tau_{z\theta}}{\partial z} + \frac{1}{r}\frac{\partial\sigma_\theta}{\partial\theta} + \frac{2\tau_{r\theta}}{r} = 0$$

$$\frac{\partial\tau_{rz}}{\partial r} + \frac{\partial\sigma_z}{\partial z} + \frac{1}{r}\frac{\partial\tau_{z\theta}}{\partial\theta} + \frac{\tau_{rz}}{r} = 0 \tag{6}$$

The linear relations between the strain and displacements are:

$$\varepsilon_z = \frac{\partial u_z}{\partial z}\ ,\ \varepsilon_\theta = \frac{u_r}{r} + \frac{1}{r}\frac{\partial u_\theta}{\partial\theta}\ \varepsilon_r = \frac{\partial u_r}{\partial r}$$

$$\gamma_{r\theta} = \frac{-u_\theta}{r} + \frac{\partial u_\theta}{\partial r} + \frac{1}{r}\frac{\partial u_r}{\partial\theta}\ ,\gamma_{zr} = \frac{\partial u_z}{\partial r} + \frac{\partial u_r}{\partial z}$$

$$\gamma_{z\theta} = \frac{\partial u_\theta}{\partial z} + \frac{1}{r}\frac{\partial u_z}{\partial\theta} \tag{7}$$

By using Eqs. (5)-(7), the following state space equations can be derived:

$$\frac{d}{dr}\delta = G\ \delta \tag{8}$$

where $\delta = \left\{\sigma_r \quad u_z \quad u_\theta \quad u_r \quad \tau_{rz} \quad \tau_{r\theta}\right\}^T$ is the state variable vector, and G is the coefficients matrix (see Appendix).

The in-plane stresses in terms of state variables are expressed as:

$$\sigma_z = \frac{Q_{13}}{Q_{33}}\sigma_r + \left(Q_{11} - \frac{Q_{13}^2}{Q_{33}}\right)\frac{\partial u}{\partial z} + \frac{1}{r}\left(Q_{12} - \frac{Q_{23}Q_{13}}{Q_{33}}\right)\frac{\partial u_\theta}{\partial\theta} + \frac{1}{r}\left(Q_{12} - \frac{Q_{13}Q_{23}}{Q_{33}}\right)u_r$$

$$\sigma_\theta = \frac{Q_{23}}{Q_{33}}\sigma_r + \left(Q_{22} - \frac{Q_{13}Q_{23}}{Q_{33}}\right)\frac{\partial u}{\partial z} + \frac{1}{r}\left(Q_{22} - \frac{Q_{23}^2}{Q_{33}}\right)\frac{\partial u_\theta}{\partial\theta} + \frac{1}{r}\left(Q_{22} - \frac{Q_{23}^2}{Q_{33}}\right)u_r$$

$$\tau_{z\theta} = Q_{66}\left(\frac{\partial u_\theta}{\partial z} + \frac{1}{r}\frac{\partial u_z}{\partial\theta}\right) \tag{9}$$

The relations for simply supported edges boundary conditions are:

$$\sigma_z = 0\ ,\ u_\theta = u_r = 0 \text{ at } \ z = 0,\ \mathrm{L}$$

$$\sigma_\theta = 0\ ,\ u_z = u_r = 0 \text{ at } \ \theta = 0,\ \theta_{\mathrm{m}} \tag{10}$$

3. Solution Procedure

In order to satisfy the simply supported boundary conditions, Eq. (10), displacement and stress components are assumed as:

$$u_r = u_r^{*}\sin\left(p_n z\right)\sin\left(p_m\theta\right)$$

$$u_z = u_z^* \cos(p_n z)\sin(p_m\theta)$$

$$u_\theta = u_\theta^* \sin(p_n z)\cos(p_m\theta)$$

$$\sigma_r = \sigma_r^* \sin(p_n z)\sin(p_m\theta)$$

$$\sigma_\theta = \sigma_\theta^* \sin(p_n z)\sin(p_m\theta)$$

$$\sigma_z = \sigma_z^* \sin(p_n z)\sin(p_m\theta)$$

$$\tau_{z\theta} = \tau_{z\theta}^* \cos(p_n z)\cos(p_m\theta)$$

$$\tau_{zr} = \tau_{zr}^* \cos(p_n z)\sin(p_m\theta)$$

$$\tau_{r\theta} = \tau_{r\theta}^* \sin(p_n z)\cos(p_m\theta) \quad (11)$$

Where $p_n = n\pi/L$, $p_m = m\pi/L$, n and m are the wave numbers along the axial and circumferential directions, respectively.

For convenience, the dimensionless physical quantities are defined by:

$$\left(\bar{\sigma}_r, \bar{\sigma}_\theta, \bar{\sigma}_z, \bar{\tau}_{r\theta}, \bar{\tau}_{zr}, \bar{\tau}_{z\theta}\right) = \left(\sigma_r^*, \sigma_\theta^*, \sigma_z^*, \tau_{r\theta}^*, \tau_{zr}^*, \tau_{z\theta}^*\right)\frac{1}{E_m}$$

$$\left(\bar{U}_r, \bar{U}_\theta, \bar{U}_z\right) = \left(u_r^*, u_\theta^*, u_z^*\right)\frac{1}{h}$$

$$\bar{z} = \frac{z}{L}, \quad \bar{r} = \frac{r}{r_i}, \quad \bar{p}_m = \theta_m p_m, \quad \bar{p}_n = L p_n$$

$$\bar{Q}_{ij} = E_m Q_{ij} \quad (12)$$

By using Eqs. (8), (11) and (12), the following state-space equations for the FG-CNTRC layer is derived

$$\frac{d}{d\bar{r}}\bar{\delta} = \bar{G}\ \bar{\delta} \quad (13)$$

where $\bar{\delta} = \{\bar{\sigma}_r \quad \bar{u}_z \quad \bar{u}_\theta \quad \bar{u}_r \quad \bar{\tau}_{rz} \quad \bar{\tau}_{r\theta}\}^T$ and $\bar{\mathrm{G}}$ is defined in the appendix.

The general solution for Eq. (13) can be explicitly expressed as:

$$\bar{\delta} = \bar{\delta}_i e^{\int_1^{\bar{r}} \bar{G} d\bar{r}} \qquad 1 \le \bar{r} \le (\bar{r}_o) \quad (14)$$

where $\bar{\delta}_i$ is $\bar{\delta}$ at $\bar{r} = 1$

Eq. (14) at $\bar{r} = \bar{r}_o$ yields:

$$\bar{\delta}(\bar{r}_o) = M\,\bar{\delta}_i \quad (15)$$

where $M = e^{\int_1^{\bar{r}_o} \bar{G} d\bar{r}}$.

Non-dimensional in-plane stresses can be derived from Eqs. (9), (11) and (12) as:

$$\bar{\sigma}_z = \frac{\bar{Q}_{13}}{\bar{Q}_{33}}\bar{\sigma}_r + \bar{p}_n\left(\frac{h}{L}\right)\left(-\bar{Q}_{11} + \frac{\bar{Q}_{13}^2}{\bar{Q}_{33}}\right)\bar{U}_z + \left(\frac{h}{r_i}\right)\left(\frac{\bar{p}_m}{\theta_m}\right)\frac{1}{\bar{r}}\left(-\bar{Q}_{12} - \frac{\bar{Q}_{23}\bar{Q}_{13}}{\bar{Q}_{33}}\right)\bar{U}_\theta + \left(\frac{h}{r_i}\right)\frac{1}{\bar{r}}\times\left(\bar{Q}_{12} - \frac{\bar{Q}_{13}\bar{Q}_{23}}{\bar{Q}_{33}}\right)\bar{U}_r$$

$$\bar{\sigma}_\theta = \frac{\bar{Q}_{23}}{\bar{Q}_{33}}\bar{\sigma}_r + \bar{p}_n\left(\frac{h}{L}\right)\left(-\bar{Q}_{12} + \frac{\bar{Q}_{13}\bar{Q}_{23}}{\bar{Q}_{33}}\right)\bar{U}_z + \left(\frac{h}{r_i}\right)\left(\frac{\bar{p}_m}{\theta_m}\right)\frac{1}{\bar{r}}\left(-\bar{Q}_{22} + \frac{\bar{Q}_{23}^2}{\bar{Q}_{33}}\right)\bar{U}_\theta + \left(\frac{h}{r_i}\right)\frac{1}{\bar{r}}\times\left(\bar{Q}_{22} - \frac{\bar{Q}_{23}^2}{\bar{Q}_{33}}\right)\bar{U}_r$$

$$\tau_{z\theta} = \left(\frac{h}{L}\right)\bar{Q}_{66}\left(\bar{p}_n\bar{U}_\theta + \frac{1}{\bar{r}}\left(\frac{\bar{p}_m}{\theta_m}\right)\left(\frac{L}{r_i}\right)\bar{U}_z\right) \quad (16)$$

Inner and outer Surfaces boundary conditions are assumed as:

$$\bar{\sigma}_r = -\bar{p}\ , \quad \bar{\tau}_{r\theta} = \bar{\tau}_{rz} = 0 \text{ at } \bar{r} = 1$$

$$\bar{\sigma}_r = 0, \quad \bar{\tau}_{r\theta} = \bar{\tau}_{rz} = 0 \text{ at } \bar{r} = \bar{r}_o \quad (17)$$

Applying surfaces tractions, Eqs. 17 to the Eq. 15, displacement components at the inner surface of the panel are obtained:

$$\begin{Bmatrix}\bar{U}_z\\ \bar{U}_\theta\\ \bar{U}_r\end{Bmatrix} = \begin{bmatrix} m_{12} & m_{13} & m_{14}\\ m_{52} & m_{53} & m_{54}\\ m_{62} & m_{63} & m_{64}\end{bmatrix}^{-1}\begin{Bmatrix} m_{11}\\ m_{51}\\ m_{61}\end{Bmatrix}\bar{p} \quad (18)$$

where m_{ii} is the element of matrix M .

By using Eqs. (18), (17.1) and (14) state variables in three dimensions can be derived. Finally by substituting the obtained state variables into the induced variable, Eq. (16) the in-plane stresses can be determined.

4. Numerical Results and Discussion

In this section a simply-supported FG-CNT cylindrical panel with the following material properties for the CNT and polymer matrix is considered to illustrate the foregoing analysis.

$E_{11}^{CN} = 5.6466^{TPa}$, $\nu_{12}^{CN} = 0.19$, $E_{22}^{CN} = E_{33}^{CN} = 7.0800^{TPa}$

$G_{12}^{CN} = G_{13}^{CN} = 1.9445^{TPa}$, $\eta_2 = \eta_3$, $\rho^{CNT} = 1.4^{[\frac{gr}{cm^3}]}$,

$E^m = 2.1^{GPa}$, $\nu^m = 0.34$, $\rho^m = 1.5^{[\frac{gr}{cm^3}]}$, $\eta_1 = 0.149$,

$\eta_2 = 0.934$

To show the effect of CNT on the bending behaviour of nanocomposite, numerical illustration is made. The effect of CNT volume fraction on the stress and displacement field at mid radius of cylindrical panel for various spans and lengths to mid radius ratio is depicted in table1. According to the table CNT inclusion in the cylindrical panel affects the mechanical entities in smaller spans as well as the smaller lengths to mid radius ratio. For further discussion, numerical investigations were carried out and presented in Figs.2-8. Figs. 2a-2e depict the effect of five cases of CNT distributions, *UD*, *FG-V*, $FG-\Lambda$, $FG-X$ and $FG-\Lambda$ on the stress and displacement field for the CNTRC cylindrical panel. According to the Figures, the transverse normal and shear stresses, $\bar{\sigma}_r$, $\bar{\tau}_{rz}$ and axial displacement, transverse displacement, $\bar{U}_z$ has minimum value in $FG-\Lambda$ case and maximum value in FG-V case where as circumferential displacement, $\bar{U}_\theta$ is not affected by the case of CNT distribution. Also it is observed that the effect of case of CNT distribution on the transverse shear stress, $\bar{\tau}_{r\theta}$ is insignificant. Henceforth, all of the numerical results are presented for the $FG-\Lambda$ case. The effect of CNT volume fraction on stress and displacement fields is presented in Figs.3a-3f. From the figures it is observed that the effect of increasing the CNT volume fraction on the transverse normal and shear stresses is not significant in comparison with the in-plane stresses. Also, from Fig.3b, it is seen that the circumferential stress decreases linearly with nearly constant value at the inner radius when the CNT volume fraction increases.

According to Fig.3c increase in the CNT volume fraction leads to increase in the axial stress nonlinearly with remaining almost constant at the outer radius. As the Figs. 3e and 3f depict, increase in the CNT volume fraction leads to decrease in the circumferential and axial displacements. Moreover, it can be observed that this effect in the circumferential displacement is more significant near the inner region whereas this effect for the axial displacement is noticeable near the outer surface.

Through the thickness distribution of stress and displacement components for various spans of the panel are depicted in Figs. 4a-4c. From the figures it is seen that increasing the span of the panel leads to change gradually the slope of the stresses and displacement distribution curves. Furthermore it can be observed that the span effect for the radial normal and transverse shear stresses at mid radius and for the axial displacement at the outer radius is more significant. The influence of internal uniformed pressure on the mechanical behaviour of nanocomposite cylindrical panel is presented in Figs.5a-5g. From the figures it is seen that the stresses and displacement increase when the applied load increases.

From the Figs.5b and 5c, it is revealed that the neutral axis along the axial and circumferential direction does not coincide with the mid surface of the cylindrical panel. Moreover it is seen that the effect of mechanical load on the axial normal stress (Fig.5b) at the outer surface is more significant while it is almost negligible at the inner surface.

As the Fig. 5c shows the influence of applied mechanical load on the circumferential stress at the inner surface is greater than that at the outer surface. Transverse shear stress, $\bar{\tau}_{rz}$ in FG-CNTRC cylindrical panel, in contrast with the isotropic cylindrical panel is not axisymmetry with respect to the mid radius (Fig.4d). Fig.5e depicts that the effect of external applied load on the in-plane shear stress at the outer surface is greater than that at the inner surface, also it is seen that this shear stress at the mid surface, without depending on the external mechanical load, is always zero. As the Figs. 5f and 5g show, increasing the external load leads to increase in the slope through the thickness distribution of axial and circumferential displacement. Also it can be concluded that the effect of external load in axial displacement at the outer radius is greater than that at the inner radius and it is converse for the circumferential displacement. Figs.6a and 6b show the influence of the CNT volume fraction on the radial and axial stresses at mid radius of thin and thick FG-CNTRC panels, respectively.

From these figures it is evident that the effect of increasing the CNT volume fraction on both radial and axial stresses in the thin panel is more considerable than that for the thick panel. Radial stress distribution along the thickness direction for the thin and thick cylindrical panels with and without containing the CNT is presented in Fig. 7.

Table1. Effect of CNT volume fraction on the stress and displacement field at mid radius of cylindrical panel with various span and length to mid radius ratio and $S = 10,\ m = n = 5$

V^*_{CNT}	ϕ	$\frac{L}{R}$	$\bar{\sigma}_r$	$\bar{\sigma}_\theta$	$\bar{\sigma}_z$	$\bar{\tau}_{rz}$	$\bar{\tau}_{r\theta}$	$\bar{U}_\theta$	$\bar{U}_z$
0.11	$\frac{\pi}{4}$	2	-0.390	-2.285	10.091	-0.874	-0.986	-1.328	2.418
		3	-0.604	-1.818	5.320	-0.850	-1.008	-1.344	6.621
		4	-0.666	-0.839	1.920	-0.730	-1.023	-1.369	8.444
	$\frac{\pi}{3}$	2	-0.389	-2.890	25.461	-0.650	-1.251	-5.442	1.448
		3	-1.106	-6.873	27.107	-0.735	-1.299	-5.519	10.166
		4	-1.534	-6.147	18.879	-0.949	-1.316	-5.561	21.771
	$\frac{\pi}{2}$	2	0.381	5.393	31.995	-0.117	-1.571	-34.718	-1.878
		3	-0.002	-5.288	56.063	0.062	-1.921	-42.435	3.567
		4	-0.843	-15.795	86.937	-0.098	-2.012	-43.794	17.381
0.14	$\frac{\pi}{4}$	2	-0.381	-3.046	11.545	-0.925	-0.994	-1.292	2.319
		3	-0.602	-2.250	6.050	-0.910	-1.017	-1.309	6.614
		4	-0.670	-1.007	2.092	-0.810	-1.031	-1.335	8.446
	$\frac{\pi}{3}$	2	-0.373	-4.618	28.649	-0.691	-1.256	-5.299	1.081
		3	-1.095	-8.901	30.869	-0.782	-1.310	-5.369	9.785
		4	-1.534	-7.591	21.370	-1.030	-1.328	-5.415	21.595
	$\frac{\pi}{2}$	2	0.382	4.475	22.977	-0.166	-1.559	-33.721	-2.500
		3	0.031	-9.050	63.155	0.071	-1.926	-41.301	2.462
		4	-0.808	-22.088	99.166	-0.091	-2.027	-42.619	16.200
0.17	$\frac{\pi}{4}$	2	-0.376	-3.779	12.951	-0.962	-1.002	-1.253	2.274
		3	-0.603	-2.640	6.683	-0.982	-1.026	-1.274	6.679
		4	-0.674	-1.136	2.182	-0.876	-1.041	-1.300	8.479
	$\frac{\pi}{3}$	2	-0.365	-6.300	31.891	-0.727	-1.264	-5.152	0.782
		3	-1.093	-10.836	34.472	-0.808	-1.322	-5.214	9.583
		4	-1.542	-8.911	23.587	-1.088	-1.341	-5.266	21.680
	$\frac{\pi}{2}$	2	0.382	3.736	23.846	-0.231	-1.556	-32.833	-3.058
		3	0.053	-12.731	70.488	0.086	-1.937	-40.173	1.500
		4	-0.799	-28.307	111.647	-0.065	-2.045	-41.409	15.344

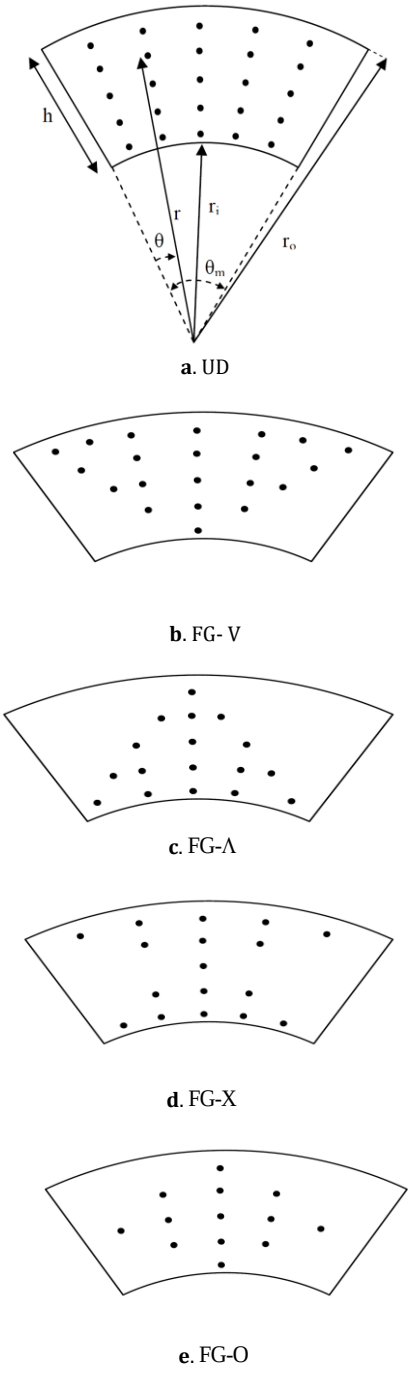

a. UD

b. FG- V

c. FG-Λ

d. FG-X

e. FG-O

Figure 1. Geometry of CNTRC

The existence of CNT in both thin and thick composite cylindrical panels leads to decrease in the radial stress; in addition, it is seen that the effect of CNT in the thin panel along the radial direction is more important than that for the thick panel.

5. Conclusions

Bending behaviour of FG-CNTRC cylindrical panel with simply supported edges and various cases of CNT distribution was examined. The governing differential equations are based on 3-D theory of elasticity. The analysis was carried out by using the Fourier series expansion along the longitudinal and circumferential directions and state space technique in the radial direction. The accuracy of the conventional two dimensional theories can be validated by this closed form solution.

From numerical illustrations the following conclusions are derived;

- Radial normal, transverse shear stresses and axial displacement in the case of $FG-\Lambda$ at a point are always smaller in magnitude than those at the corresponding points in the other two cases of CNT distribution.
- The existence of CNT in cylindrical panel decreases the axial and circumferential displacement components as well as the normal and shear stresses in radial and circumferential directions.
- The effect of CNT volume fraction on the axial displacement in contrast with the circumferential displacement at the outer radius is more significant while it is negligible at the inner radius
- The influence of external load on the axial displacement In contrast with the circumferential displacement at outer radius is more noticeable.
- The effect of CNT volume fraction on the bending behaviour of the thin FG-CNTRC cylindrical panel is more significant than that for the thick panel.

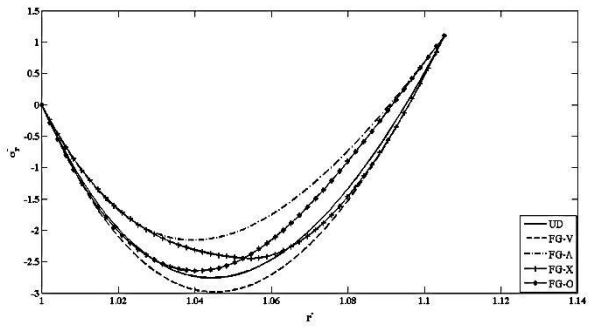

a. Radial normal stress

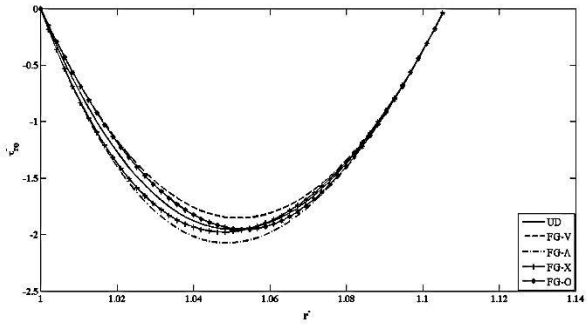

b. Transverse shear stress

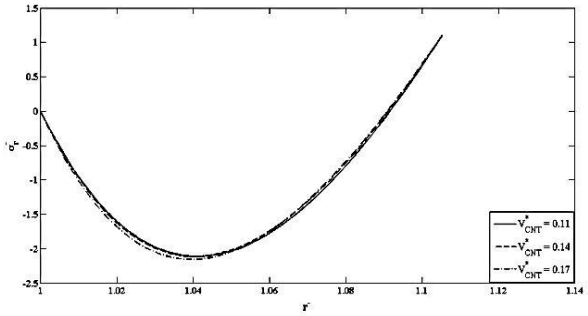

a. Radial normal stress

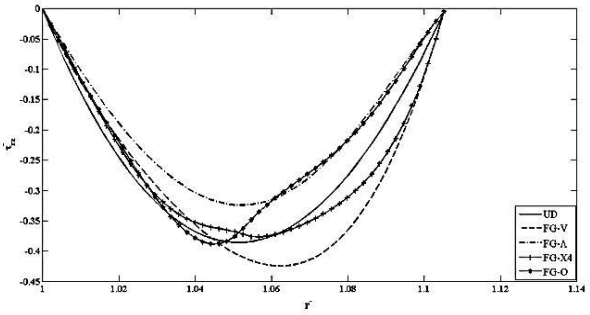

c. Transverse shear stress

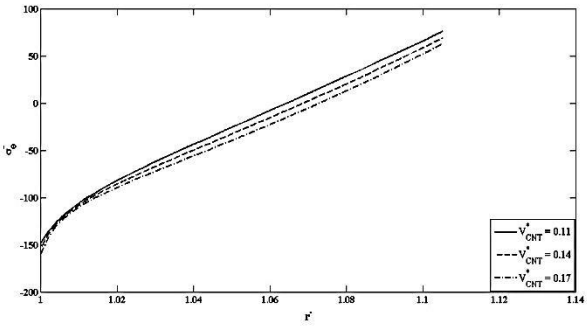

b. Circumferential normal stress

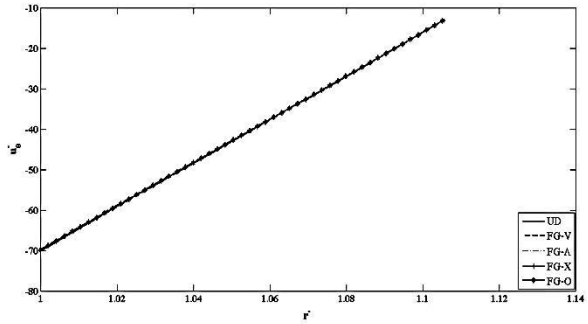

d. Circumferential displacement

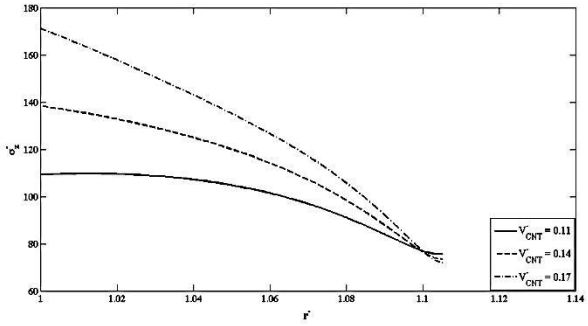

c. Axial normal stress

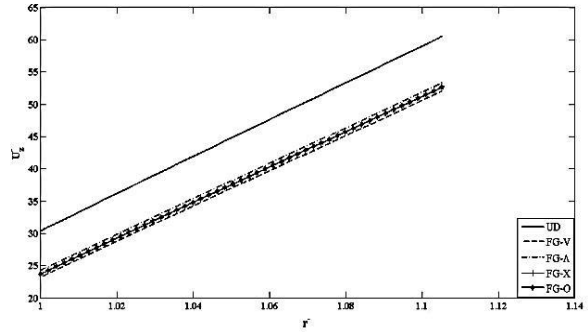

e. Axial displacement

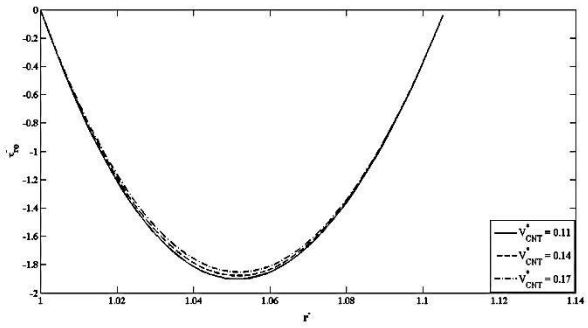

d. Transverse shear stress

Figure 2. Distribution of mechanical entities along the thickness for various cases of CNT distribution for the cylindrical panel with V^{*}_{CNT} =0.17, m = n=25

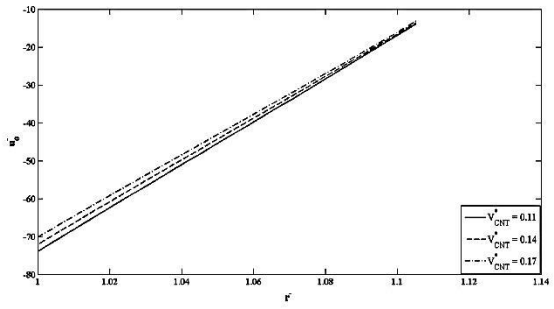

e. Circumferential displacement

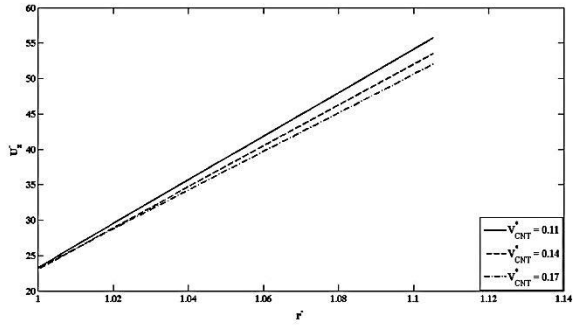

f. Axial displacement

Figure 3. Effect of CNT volume fraction on the through the thickness stresses and displacements for the FG − Λ CNTRC cylindrical panel , with L/h = 50, $V^*_{CNT} = 0.17$

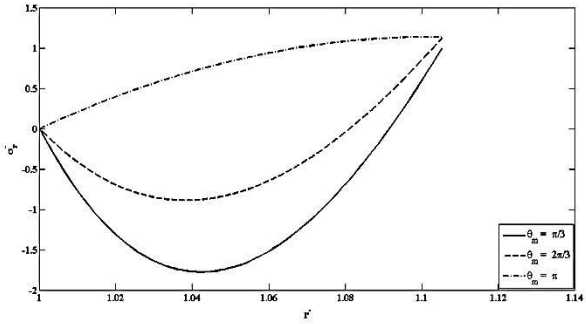

a. Radial normal stress

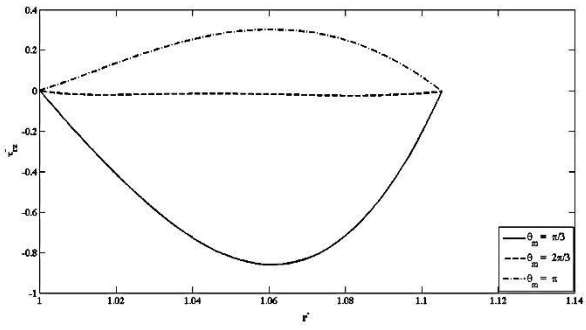

b. Transverse shear stress

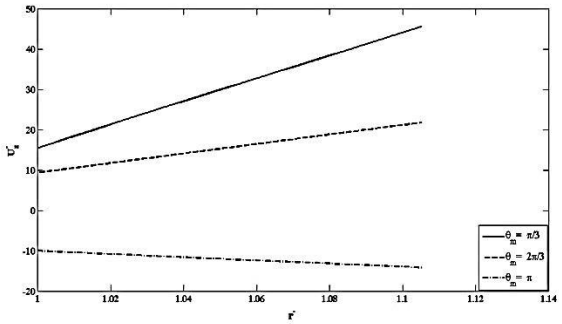

c. Axial displacement

Figure 4. Effect of span of panel on the through the thickness distribution of stresses and displacements for the FG-V CNTRC hybrid beam, with L/h = 50, $V^*_{CNT} = 0.17$

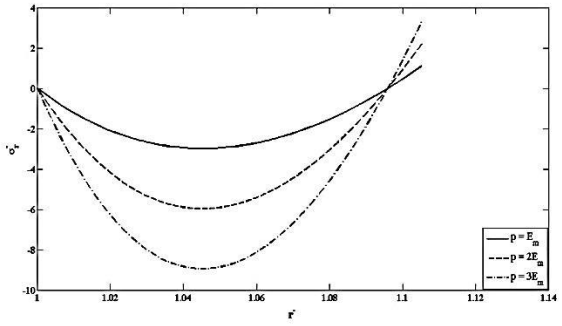

a. Radial normal stress

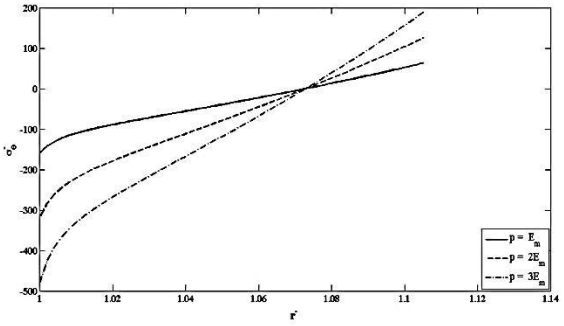

b. Circumferential normal stress

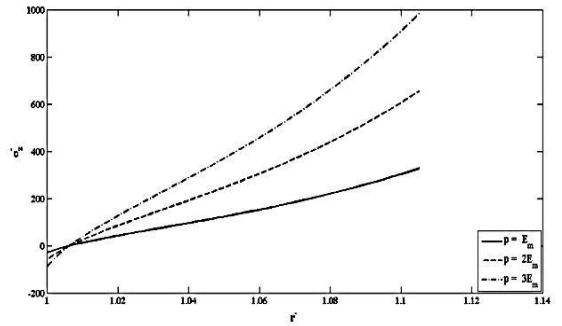

c. Axial normal stress

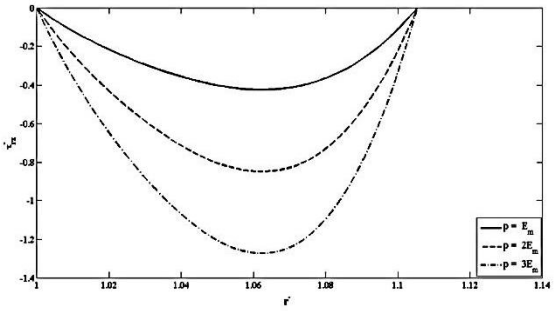

d. Transverse shear stress

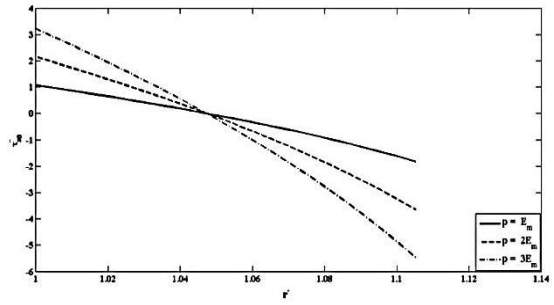

e. In-plane shear stress

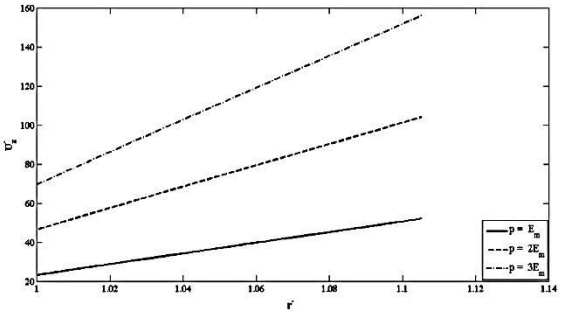

f. Axial displacement

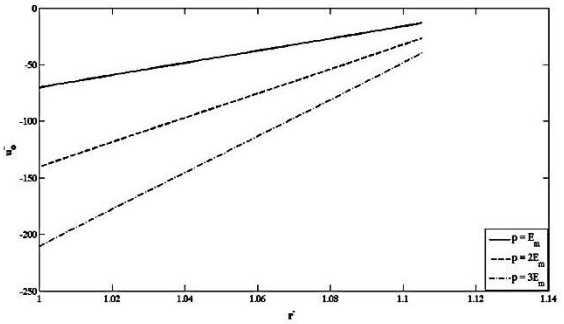

g. Circumferential displacement

Figure 5. Effect of internal pressure on the through the thickness distribution of stresses, displacements for the FG-CNTRC hybrid beam with L/h = 50, $V^*_{CNT} = 0.17$

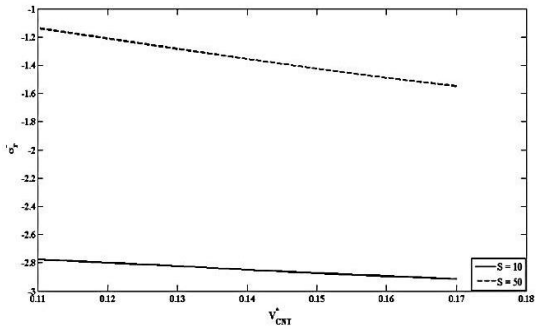

a. Radial normal stress

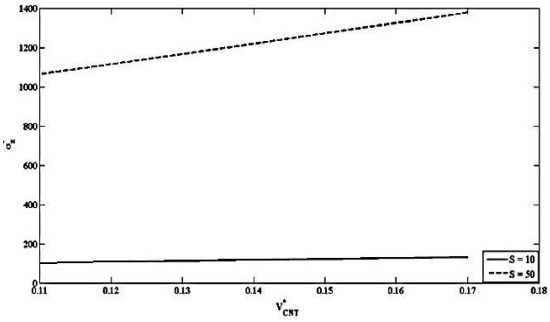

b. Axial normal stress

Figure 6. Effect of increasing the CNT volume fraction on radial and axial normal stresses at mid surface of the thick and thin panels for the FG-V CNTRC

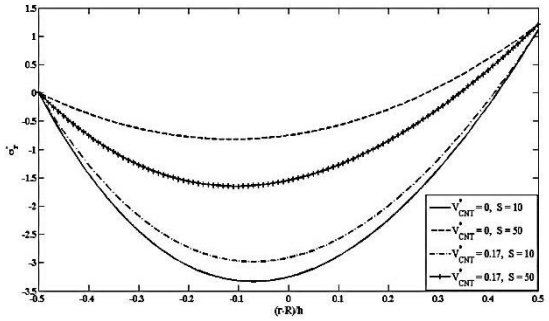

Figure 7. Distribution of radial stress for the thick and thin panels with and without the CNT

Nomenclature

E_{11}^{CN} , E_{22}^{CN} , G_{12}^{CN} , E^m , G^m	Young's modulus, shear modulus, shear modulus of carbon nano-tube and matrix respectively
V_{CN} , V_m	volume fractions of carbon nano-tube and matrix, respectively
h , L	thickness and axial length of the panel
W_{CN} , ρ_{CN} ,	mass fraction and density fraction of CNT, respectively

ρ_m	density fraction of matrix
$\sigma_i (i=r,\theta,z)$	normal stresses
$\tau_{z\theta}$, $\tau_{r\theta}$, τ_{rz}	shear stresses
$\eta_i \ (i=1,2,3)$	efficiency parameter of CNT
δ	state variables
n, m	half wave numbers in the x- and y-directions
u_r, u_θ, u_z	displacements in the r- , θ - and z-directions, respectively
$\gamma_{r\theta}, \gamma_{rz}, \gamma_{z\theta}$	shear strains
$\varepsilon_i (i=r,\theta,z)$	normal strains

Appendix

$$Q_{11}=\frac{E_{11}}{\Delta}\left(1-\nu_{23}\nu_{32}\right),\ Q_{22}=\frac{E_{22}}{\Delta}\left(1-\nu_{31}\nu_{13}\right)$$

$$Q_{33}=\frac{E_{33}}{\Delta}\left(1-\nu_{12}\nu_{21}\right)\ Q_{44}=G_{23}\ Q_{55}=G_{13}\ Q_{66}=G_{12}$$

$$Q_{12}=\frac{E_{11}}{\Delta}\left(\nu_{21}+\nu_{31}\nu_{23}\right)\ Q_{13}=\frac{E_{11}}{\Delta}\left(\nu_{31}+\nu_{21}\nu_{32}\right)$$

$$Q_{23}=\frac{E_{22}}{\Delta}\left(\nu_{32}+\nu_{12}\nu_{31}\right)$$

$$\Delta=1-\nu_{12}\nu_{21}-\nu_{23}\nu_{32}-\nu_{31}\nu_{13}-2\nu_{12}\nu_{32}\nu_{13}$$

$$G=\begin{bmatrix} \frac{a_1}{r} & \frac{a_2}{r}\frac{\partial}{\partial z} & \frac{a_3}{r^2}\frac{\partial}{\partial\theta} & \frac{a_3}{r^2} & -\frac{\partial}{\partial z} & -\frac{\partial}{\partial\theta} \\ 0 & 0 & 0 & -\frac{\partial}{\partial z} & a_4 & 0 \\ 0 & 0 & \frac{1}{r} & -\frac{1}{r}\frac{\partial}{\partial\theta} & 0 & a_5 \\ a_6 & -a_7\frac{\partial}{\partial z} & \frac{-a_8}{r}\frac{\partial}{\partial\theta} & \frac{-a_8}{r} & 0 & 0 \\ -a_7\frac{\partial}{\partial z} & a_{11} & -\frac{a_{10}}{r}\frac{\partial^2}{\partial z\,\partial\theta} & \frac{-a_2}{r} & -\frac{1}{r} & 0 \\ \frac{-a_8}{r}\frac{\partial}{\partial\theta} & \frac{a_{10}}{r}\frac{\partial^2}{\partial z\,\partial\theta} & a_{12} & -\frac{a_3}{r^2}\frac{\partial}{\partial\theta} & 0 & -\frac{2}{r} \end{bmatrix}$$

where

$$a_1=\left(\frac{Q_{23}}{Q_{33}}-1\right)\quad a_2=\left(Q_{12}-\frac{Q_{13}Q_{23}}{Q_{33}}\right)\quad a_3=\left(Q_{22}-\frac{Q_{23}^2}{Q_{33}}\right)$$

$$a_4=\frac{1}{Q_{55}}\quad a_5=\frac{1}{Q_{44}}\quad a_6=\frac{1}{Q_{33}}\quad a_7=\frac{Q_{13}}{Q_{33}}\quad a_8=\frac{Q_{23}}{Q_{33}}$$

$$a_9=\left(Q_{11}-\frac{Q_{13}^2}{Q_{33}}\right)\ a_{10}=\left(Q_{12}+Q_{66}-\frac{Q_{23}Q_{13}}{Q_{33}}\right)$$

$$a_{11}=-a_9\frac{\partial^2}{\partial z^2}-\frac{Q_{66}}{r^2}\frac{\partial^2}{\partial\theta^2}\qquad a_{12}=Q_{66}\frac{\partial^2}{\partial z^2}-\frac{a_3}{r^2}\frac{\partial^2}{\partial\theta^2}$$

$$\bar{G}=\begin{bmatrix} \frac{\bar{a}_1}{\bar{r}} & \frac{\bar{a}_2}{\bar{r}} & \frac{\bar{a}_3}{\bar{r}^2} & \frac{\bar{a}_3'}{\bar{r}^2} & \bar{p}_n\frac{r_i}{L} & \frac{\bar{p}_m}{\theta_m}\frac{1}{\bar{r}} \\ 0 & 0 & 0 & -\bar{p}_n\frac{r_i}{L} & \bar{a}_4 & 0 \\ 0 & 0 & \frac{1}{\bar{r}} & -\frac{1}{\bar{r}}\frac{\bar{p}_m}{\theta_m} & 0 & \bar{a}_5 \\ \bar{a}_6 & \bar{a}_7 & \frac{\bar{p}_m}{\theta_m}\frac{\bar{a}_8}{\bar{r}} & \frac{-\bar{a}_8}{\bar{r}} & 0 & 0 \\ -\bar{a}_7 & \bar{a}_9-\frac{\bar{a}_9'}{\bar{r}^2} & \frac{\bar{a}_{10}}{\bar{r}} & \frac{-\bar{a}_2}{\bar{r}} & -\frac{1}{\bar{r}} & 0 \\ \frac{-\bar{a}_8}{\bar{r}} & \frac{\bar{a}_{10}}{\bar{r}} & a_{13} & \frac{\bar{a}_3}{\bar{r}^2} & 0 & -\frac{2}{\bar{r}} \end{bmatrix}$$

$$a_{13}=\bar{p}_n^2\frac{r_i}{L}\frac{h}{L}\bar{Q}_{66}-\frac{\bar{p}_m}{\theta_m}\frac{\bar{a}_3}{\bar{r}^2}\quad \bar{a}_1=\left(\frac{\bar{Q}_{23}}{\bar{Q}_{33}}-1\right)$$

$$\bar{a}_2=\bar{p}_n\left(\frac{h}{L}\right)\left(\frac{\bar{Q}_{13}\bar{Q}_{23}}{\bar{Q}_{33}}-\bar{Q}_{12}\right)$$

$$\bar{a}_3=\left(\frac{\bar{p}_m}{\theta_m}\right)\left(\frac{h}{r_i}\right)\left(-\bar{Q}_{22}+\frac{\bar{Q}_{23}^2}{\bar{Q}_{33}}\right)$$

$$\bar{a}_3'=\left(\frac{h}{r_i}\right)\left(\bar{Q}_{22}-\frac{\bar{Q}_{23}^2}{\bar{Q}_{33}}\right)\ \bar{a}_4=\left(\frac{r_i}{h}\right)\frac{1}{\bar{Q}_{55}}\quad \bar{a}_5=\left(\frac{r_i}{h}\right)\frac{1}{\bar{Q}_{44}}$$

$$\bar{a}_6=\left(\frac{r_i}{h}\right)\frac{1}{\bar{Q}_{33}}\quad \bar{a}_7=\left(\frac{r_i}{L}\right)\bar{p}_n\frac{\bar{Q}_{13}}{\bar{Q}_{33}}\quad \bar{a}_8=\left(\frac{\bar{p}_m}{\theta_m}\right)\frac{\bar{Q}_{23}}{\bar{Q}_{33}}$$

$$\bar{a}_9=\bar{p}_n^2\left(\frac{r_i}{L}\right)\left(\frac{h}{L}\right)\left(\bar{Q}_{12}-\frac{\bar{Q}_{13}^2}{\bar{Q}_{33}}\right)\ \bar{a}_9'=\left(\frac{\bar{p}_m}{\theta_m}\right)^2\frac{h}{r_i}\bar{Q}_{66}$$

$$\bar{a}_{10}=\left(\frac{h}{L}\right)\left(\frac{\bar{p}_m\bar{p}_n}{\theta_m}\right)\left(\bar{Q}_{12}+\bar{Q}_{66}-\frac{\bar{Q}_{23}\bar{Q}_{13}}{\bar{Q}_{33}}\right)$$

References

[1] Thostenson, ET, Ren,ZF, Chou, TW. Advances in the science and technology of carbon nanotubes and their composite: a review, Compos Sci Thecnol 2001; 61:1899-912.

[2] Gou J, Minaie B, Wang B, Liang Z, Zhang C. Computational and experimental study of interfacial bonding of single-walled nanotube re-

inforced composites stiffness, Comp Mater Sci 2004;31:225–236.
[3] Wuite J, Adali S. Deflection and stress behavior of nanocomposite reinforced beams using a multi scale analysis, Compos Struct 2005;71:388–396.
[4] Vodenitcharova T, Zhang C. Bending and local buckling of a nanocomposite beam reinforced by a single-walled carbon nanotube, Int J Sol Struct 2006; 43:3006–3024.
[5] Shen HS. Nonlinear bending of functionally graded carbon nanotube-reinforced composite plates in thermal environments, Compos Struct 2009;91:9–19.
[6] Formica G, Lacarbonara W, Alessi R. Vibrations of carbon nanotube-reinforced composites, Sound Vib 2010;329:1875–1889.
[7] Shen HS, Zhang C. Thermal buckling and post buckling behavior of functionally grade carbon nanotube-reinforced composite plates, Mater Design 2010;31:3403–3411.
[8] Ke LL, Yang J, Kitipornchai S. Nonlinear free vibration of functionally graded carbon nanotube-reinforced composite beams, Compos Struct 2010;92:676-683.
[9] Shen HS. Post buckling of nanotube-reinforced composite cylindrical shells in thermal environments, Part I: Axially-loaded shells, Compos Struct 2011; 93: 2096–2108.
[10] Shen HS. Post buckling of nanotube-reinforced composite cylindrical shells in thermal environments, Part II: Pressure-loaded shells, Compos Struct 2011;93: 2496–2503.
[11] Wang ZX, Shen HS. Nonlinear vibration of nanotube-reinforced composite plates in thermal environments, Comp Mater Sci 2011;50: 2319–2330.
[12] Mehrabadi SJ, Sobhani Aragh B, Khoshkhahesh V, Taherpour A. Mechanical buckling of nanocomposite rectangular plate reinforced by aligned and strait single-walled carbon nanotubes, Compos Part B-Eng 2012;43(4):2031-2040.
[13] Zhu P, Lei ZX, Liew KM. Static and free vibration analyses of carbon nanotube-reinforced composite plates using finite element method with first order shear deformation plate theory, Compos Struct 2012;94:1450–1460.
[14] Wang ZX, Shen HS. Nonlinear vibration and bending of sandwich plates with nanotube-reinforced composite face sheets, Compos Part B-Eng 2012;43:411–421.
[15] Yas MH, Heshmati M. Dynamic analysis of functionally graded nanocomposite beam reinforced by randomly oriented carbon nanotube under the action of moving load, Appl Math Model 2012;36:1371–1394.
[16] Alibeigloo A. Static analysis of functionally graded carbon nanotube-reinforced composite plate embedded in piezoelectric layers by using theory of elasticity, Compos Struct 2013;95:612-622.
[17] Bhardwaj G, Upadhyay AK, Pandey R, Shukla KK. Non-linear flexural and dynamic response of CNT reinforced laminated composite plate, Compos Part B-Eng 2013;45:89-100.
[18] Shen HS. Thermal buckling and post buckling behavior of functionally graded carbon nanotube-reinforced composite cylindrical shells, Compos Part B-Eng 2012; 43:1030-1038.
[19] Shen HS, Xiang Y. Nonlinear vibration of nanotube-reinforced composite cylindrical shells in thermal environments, Comput. Methods Appl. Mech. Eng 2012; 213-216:196–205.
[20] Moradi-Dastjerdi R, Foroutan M, Pourasgha A. Dynamic analysis of functionally graded nanocomposite cylinders reinforced by carbon nanotube by a mesh-free method, Mater Design 2013;44:256–266.
[21] Moradi-Dastjerdi R, Foroutan A, Pourasgha A. Eshelby–Mori–Tanaka approach for vibrational behavior of continuously graded carbon nanotube-reinforced cylindrical panels. Compos Part B-Eng 2012;43:1943–1954.